RESEARCH ARTICLE | MARCH 05 2026

Preparation and study of the annealing temperature, optical and structural properties of $ZnTe_{0.8}Se_{0.2}$ thin films FREE

Zainab Assif Abdullah; Ayad Ahmed Salih

AIP Conf. Proc. 3486, 240001 (2026)
https://doi.org/10.1063/12.0042858

Preparation and Study of the Annealing Temperature, Optical and Structural Properties of $ZnTe_{0.8}Se_{0.2}$ Thin Films

Zainab Assif Abdullah[1, a)] and Ayad Ahmed Salih[2, b)]

[1] *University of Technology, Baghdad, Iraq*
[2] *Department of Physics – College of Ibn Al-Haytham – University of Baghdad, Baghdad, Iraq*

[a)] *Zainab.a.abdulla@uotechnology.edu.iq*
[b)] *Corresponding author: ayad.a.s@ihcoedu.uobaghdad.edu.iq*

Abstract: The optical and structural characteristics of $ZnTe_{1-0.2}Se_{0.2}$ (ZTS) semiconductors are examined using the thermal evaporation process. We analyze 500 nm thickness films and explore the effects of annealing temperatures ranging from RT to 373 and 473K. The optical properties of films were assessed using a wavelength range (400-1000nm). $ZnTe_{0.8}Se_{0.2}$ semiconductors exhibit direct band gaps of 1.86, 1.81, and 1.78eV, respectively. Included in the computed optical constant are the refractive index and extinction coefficient. XRD and AFM studies demonstrate that films are polycrystalline with a superior stoichiometric composition. One of the preferred orientations of the polycrystalline phase is along the (111) direction. Also, increasing the annealing temperature led to an increase in the crystal and grain size, which contributes to improving the structural properties of the films. Additionally, the energy gap of the annealed films is close to the green color in the visible spectrum, making them suitable for optoelectronic applications.

Keywords: ZnTe0.8Se0.2, Thin Film, Optical Properties, XRD, AFM

INTRODUCTION

Chalcogenide thin films have remarkable optical properties qualities such a broad band gap and good chemical and thermal stability, which make them appealing for use in scientific research in areas like optical communication, laser power delivery, optoelectronic devices, etc.[1,2] Because of their large band gap, semiconducting thin films of II–VI group compounds are important in optoelectronic devices such as photovoltaic conversion, IR lasers, thin film transistors, blue–green light-emitting diodes, and light detecting devices.[3,4] It was observed that the energy gap of (ZnTe) at room temperature is about (2.5) electron volts [5]. As for zinc telluride, its energy gap ranges from 2 to 2.25 electron volts [6]. Significant semiconducting chalcogenide compounds, the binary compounds RX (R = Zn, Cu, Cd, Ge, Ga; X = Se, Te, S) have been described elsewhere in terms of their structural, morphological, optical, electrical, and dielectric properties [7–9]. Changing the proportions of the three elements leads to change their intrinsic properties, including crystal structure and optical properties [10,11] Chemical, physical, and cathode sputtering deposition techniques can all be used to create thin films. Such as chemical bath deposition [12], thermal evaporation under vacuum [13], electron beam evaporation [14],) sputtering [15], electron beam evaporated [16], pulsed laser deposition [17], The thermal evaporation technique is one of these efficient ways to make the thin films at ambient temperature [18] . This study examines the impact of annealing at (473,573) K on optical and structural parameters as well as their correlation. ZnTe0.8Se0.2 thin films were deposited by vacuum evaporation.

MATERIALS AND METHODS

An alloy of Zinc, Tellurium and Selenium has been produced in thin films form. The $ZnTe_{1-x}Se_x$ (ZTS) elements' high elemental purity (99.99%) and stoichiometric weight ratios (1:0.8:0.2) were combined. It was placed under pressure (1×10^{-3} mbar) in evacuated quartz tubes. It was then placed in an electric furnace at a temperature of (1273) K for six hours. After that, the alloy was removed from the furnace for a full day until it cooled gradually. After that, the alloy was crushed into powder. The melting point of the alloy (ZTS) is lower than the temperature required for the alloy to solidify according to the phase diagram.[19] The ZTS thin films (500 nm thick) were deposited onto glass substrates at room temperature using the thermal evaporation method at a pressure of $4.5x10^{-5}$ Torr and a deposition rate of 5.1 nm/s. AFM and X-ray diffraction (XRD) have been employed to ascertain the morphology (structure) of $ZnTe_{0.8}Se_{0.2}$ film. To find (XRD) patterns, a (LabX-XRD-6000 SHIMADZU Japan) with radiation λ = 1.5406 Å Cu (Kα) was utilized. For the purpose of examining the optical and structural characteristics of $ZnTe_{0.8}Se_{0.2}$ thin films, the

Technologies and Materials for Renewable Energy, Environment and Sustainability
AIP Conf. Proc. 3486, 240001-1–240001-8; https://doi.org/10.1063/12.0042858
Published under an exclusive license by AIP Publishing. 978-0-7354-5336-4/$30.00

prepared sample must be homogeneous, cling to the substrate, and not crack. Scherer's Formula was utilized to calculate the crystallite size depending on the film thickness after analyzing the X-ray diffraction of these films.[20].

$$C.S = \frac{(0.9)\,\lambda}{(\beta)\cos\,\theta} \tag{1}$$

Where the diffraction width of the peaks at half maximum is written by β (FWHM). measured the size of the crystallite (C.S.) and the diffraction maximum angle (θ). The following equation is used to get the lattice constant (a).[21].

$$\frac{1}{d^2} = \frac{(h^2 + k^2 + l^2)}{a^2} \tag{2}$$

Where (a) were the lattice constants and (hkℓ) was the number of Miller indices. The micro strain (Ɛ) for developed thin films can be found using the following formula [22].

$$\varepsilon = \frac{\beta\,(\cos\theta)}{4} \tag{3}$$

The density of dislocations (δ) is defined as a proportion of the displacement line lengths to the crystal volume. It can be determined through the equation provided below [23].

$$\delta = \frac{1}{(C.S)^2} \tag{4}$$

A double-beam spectrophotometer (EMCLAB-61PC, UV-visible) was utilized to measure light transfer between 400 and 1000 nm in wavelength. Transmission and absorption spectra covering this length range were used for determining the energy gap, and the optical properties of thin-film manufacturing were examined.
The Lambert law and the Tauc equations, respectively, have been used to derive (Eg) from the absorption spectra. [24].

$$\alpha = (2.303)\frac{A}{t} \tag{5}$$

$$\alpha h\upsilon = D\,(h\upsilon - E_g)^r \tag{6}$$

The coefficient of absorption is represented by α, the type of optical transition is given by r, and the energy amount of the incident photons is shown by hυ. Thickness (t) and absorption (A).
The coefficient of extinction k, refractive index n, and reflection R are variables that can be employed to calculate optical constants.[25].

$$k = \frac{\alpha\,\lambda}{4\pi} \tag{7}$$

$$n = \left[\frac{4R}{(1-R)^2} - k^2\right]^{1/2} + \frac{(1+R)}{(1-R)} \tag{8}$$

RESULT AND DISCUSSION

A UV/Visible (1800) spectrophotometer was utilized to measure optical transmission. The band gap of the transparent film was discovered by analyzing their optical transmission spectra (Eg) Detecting traces of absorbance and transmission in the 400–1000 nm range is made possible by the concept to generate the transmission curve (nm) as function of the wavelength, which appears over the wavelength in Figure 1. This suggests that the visible spectrum regions of $ZnTe_{0.8}Se_{0.2}$ thin films at R.T. and (373,473) K have a high absorption near 87% After post-annealing, thin films have been observed to show lower transmittance and higher absorption values. The absorption of photons by free carriers causes this increase. As a result, the transmittance lowers. On the other hand, it can be connected to the expansion of crystal size [26, 27]. As a result, lower-energy photons may be absorbed. As the annealing temperature advances, the absorption edge moves toward longer wavelengths, showing as the smaller band gap is caused by higher annealing temperatures. The absorption coefficient is significantly impacted by the band gap.

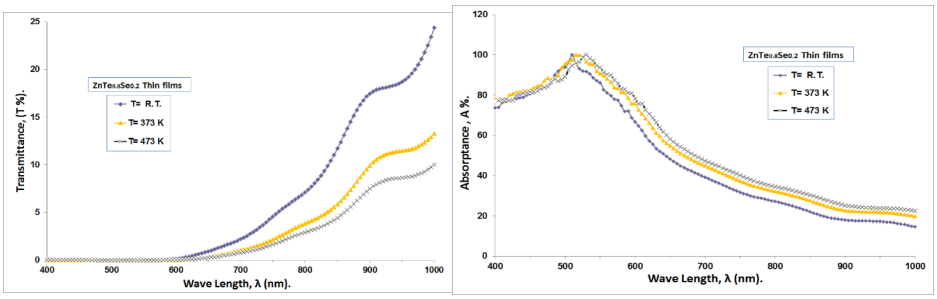

FIGURE 1. Transmittance and absorption spectrum of $ZnTe_{0.8}Se_{0.2}$ at (R.T, 373 and 473) K

For several annealing temperatures, Figure 2 displays the optical absorption coefficient as a function of wave length. However, Equation (5) can also be used to get the thin film's absorption coefficient (α) given its thickness (t) using the transmittance spectrum.

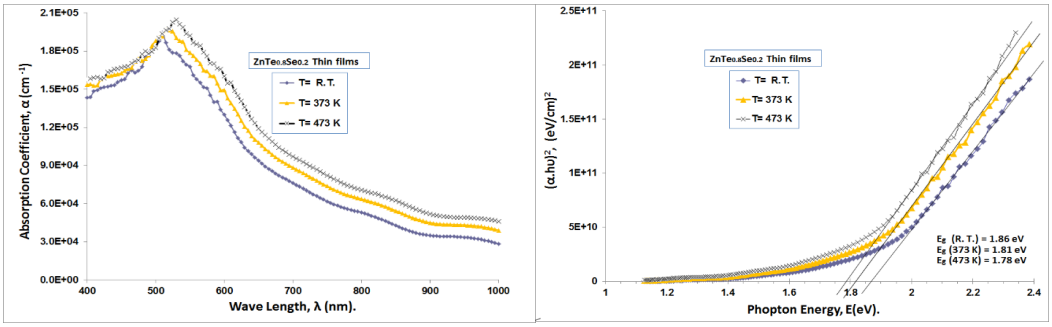

FIGURE 2. Variation in the absorption coefficient with λ for ZnTe0.8Se0.2 at temperature (R.T, 373 and 473)

The absorption coefficient values calculated here fall within the range of 10^5 cm^{-1}. A significant chance of permitted direct transitions can be seen by Figure 2, which shows that the absorption coefficient (α) approaches high levels at higher photon energies. α gradual drops as the wavelength grows. The effect of the annealing temperature on the $ZnTe_{0.8}Se_{0.2}$ film's carrier concentration and crystallinity may have an on this variance. The optical band gap is obtained using equation (6). The parameter (r), an index connected with the nature of the material given by the optical transition involved in the absorption process, specifies the permissible direct (r = 1/2). To calculate the optical energy gap of the prepared and annealed films from Figure 2 above, illustrates the extrapolation of the $(\alpha h\nu)^2$ versus (hν) plot curve's straight-line segment [28,29]. The intercept on the photon energy axis was used to determine Eg. We discovered that the direct band gap material class embraces all $ZnTe_{0.8}Se_{0.2}$ thin films and the energy gap decreases from 1.86 eV to 1.78 eV, as Table 1 was filled in with strong accords with [28]

TABLE 1. Optical parameters of (E_g^{opt}, α, n, k) at (R.T, 373, and 473) K

Thickness (500 nm)	$\mathbf{E_g^{opt}}$(eV)	α × 10^4 (cm^{-1})	n	k
R. T	1.86	16.758	1.778	0.733
373	1.81	17.864	1.658	0.782
473	1.78	19.223	1.516	0.841

The optical constants, which are essential fundamental features of matter, totally characterize the optical behavior of materials. The refractive index (n) and the extinction coefficient (k) were examples of optical constants.(24,29) Based on the discovered absorption coefficients α, the extinction coefficient k was determined by formula (7)

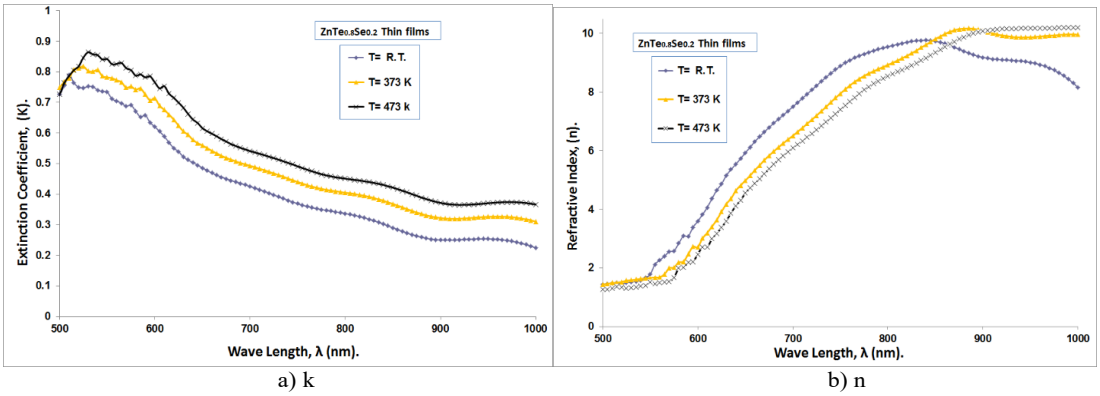

a) k b) n

FIGURE 3a,b. Variation of the optical parameters k, n versus wavelength for ZnTe0.8Se0.2 at temperature R.T, 373 and 473 K

We find that the extinction coefficient grows progressively with increasing photon energy at annealing temperatures, and then rises sharply at high photon energies. It means an increase in absorption, which raises the absorption coefficient. It observes that the curves generally show the same pattern as described earlier, with the absorption edge shifting in the direction of low photon energy. This demonstrates that the extinction coefficient is clearly increased by the annealing temperatures. Additionally, it is shown that k changes dramatically with annealing temperature before the Eg values of the films due to structural changes in the films. Figure 3 illustrates the variation in refractive index as a function of wavelengths at (R.T., 373, and 473) K. Due to its major importance in optical communication and the development of devices for spectrum dispersion, the refractive index dispersion is crucial to the study of optical materials.[24]. The refractive index values of the films were determined by Equation (8). The refractive index curve and the form of reflection are quite comparable. Based on the link between reflexive index and reflection, Table 3 gives the refractive index value for each film with a constant wavelength of 550 nm (within the visible range). The decrease in refractive index values is caused by a fall in corresponding reflection caused by molecular and compositional changes that happen throughout the annealing process. Additionally, as the refractive index drops when the energy of incoming photons above the Eg value, Figure 3 demonstrates that all of the films exhibit anomalous dispersion. Due to the plotted refractive index data, the visible region's refractive index drops as temperature rises. Free carriers in semiconductors and free electrons in metals both serve as dielectrics and absorb light [25, 26]. Figure 4 indicates the annealed and without annealed X-ray diffraction (XRD) patterns of $ZnTe_{0.8}Se_{0.2}$ thin films.

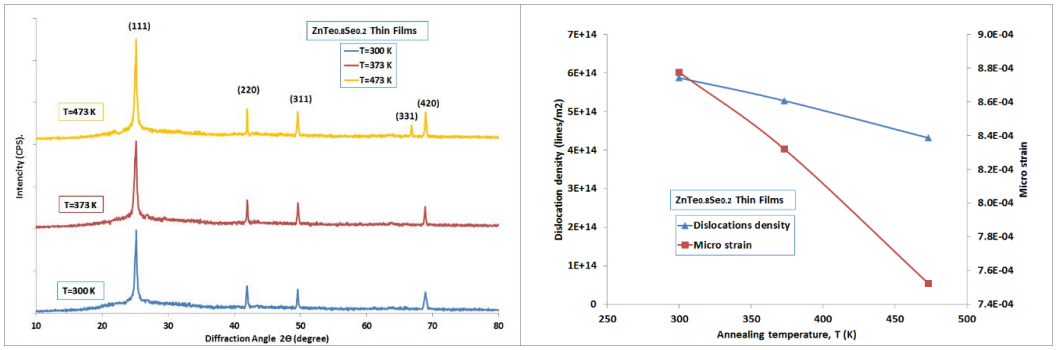

a **b**

FIGURE 4a,b. X-ray diffraction for the ZnTe thin films at (R.T, 373 K and 473 K)

The multi-diffraction peaks of the (111), (220), (311) (331) and (420) planes demonstrate the polycrystalline form of the ZTS film compound in cubic structure using the card standard value and JCPDS file number 00-015-0746. The cubic structure of the crystal is represented by the XRD peaks the films demonstrate that the favored development

direction aligns with plane (111). $ZnTe_{0.8}Se_{0.2}$ which is a ternary compound, may be linked to each diffraction peak in the JCPDS file. The films' diffraction peak positions were unchanged after annealing at 373 and 473 K, while the peak intensity and crystalite size (C.S.) increased. It showed greater regularity in the crystal structure and decreased weaknesses, indicating improved crystalline film quality. The Scherrer equation, which depends on the FWHM of the (111) peak, can be used to determine the crystallite size of the film displayed in Figure 4.

TABLE 2. X-ray diffraction results for $ZnTe_{0.8}Se_{0.2}$ thin films at various annealing T. (R.T, 373 and 473) K.

Ta (K)	$\mathbf{d_{exp.}}$ (Å)	2θexp (deg)	(**hkl**)	FWHM (deg)	C.S (nm.)	$\delta \times 10^{14}$ (lines/m2)	$\varepsilon \times 10^{-3}$
R. T	3.53268	25.189	(111)	0.2062	41.252	5.876	0.877
	2.15333	41.921	(220)				
	1.83644	49.600	(311)				
	1.36149	68.912	(420)				
373	3.53613	25.164	(111)	0.1955	43.508	5.282	0.832
	2.15230	41.942	(220)				
	1.83571	49.621	(311)				
	1.36205	68.880	(420)				
473	3.53696	25.158	(111)	0.1768	48.109	4.320	0.752
	2.15176	41.953	(220)				
	1.83710	49.581	(311)				
	1.39895	66.820	(331)				
	1.36065	68.961	(420)				

As the annealing temperature increases, the crystallite size shows a noticeable rise, as summarized in Table 2. This increase indicates an enhanced tendency of the material to crystallize, resulting in improved structural ordering within the film. The experimentally obtained lattice spacing values *d* and lattice constants *a* are found to be in very good agreement with the corresponding standard JCPDS values, confirming the formation of the expected crystalline phase and validating the accuracy of the structural analysis. This enhanced crystallinity at an annealing temperature of T_a = 473 K has a significant influence on the electrical, optical, and thermoelectric performance of the $ZnTe_{0.8}Se_{0.2}$ (ZTS) thin films. As the annealing temperature increases, structural defects such as microstrain, dislocations, and grain-boundary irregularities tend to diminish. This reduction in defects contributes to a more ordered crystal structure, which typically improves charge-carrier mobility, reduces scattering centers, and enhances optical transparency and thermoelectric efficiency. To further investigate the evolution of the film morphology, AFM surface scans were performed. Surface micro-roughness is an essential criterion for optical coatings, as it affects light scattering, absorption, and reflection. The root mean square (RMS) roughness in particular provides a quantitative measure of the surface quality and uniformity under analysis [21]. The morphological parameters extracted from the AFM images—roughness height, RMS roughness, and average grain size (G.S.)—are listed in Table 3. Across the series of annealed samples, the average grain size increased from 78.59 nm to 99.12 nm, accompanied by noticeable variations in both roughness and RMS values. This increase in surface roughness enhances the potential applicability of the films as anti-reflection coatings, which benefit from controlled micro-texturing that promotes light trapping, increases absorption, and reduces reflectance in the visible spectral region. Notably, the ZTS sample annealed at 473 K exhibits the most pronounced morphological features. This behavior can be attributed to the increased atomic mobility at higher temperatures, which facilitates grain growth, particle coalescence, and aggregation—particularly among larger grains. The trends observed through AFM measurements are consistent with the structural conclusions derived from XRD analysis, demonstrating a clear correlation between annealing-induced crystallinity and surface morphology [27].

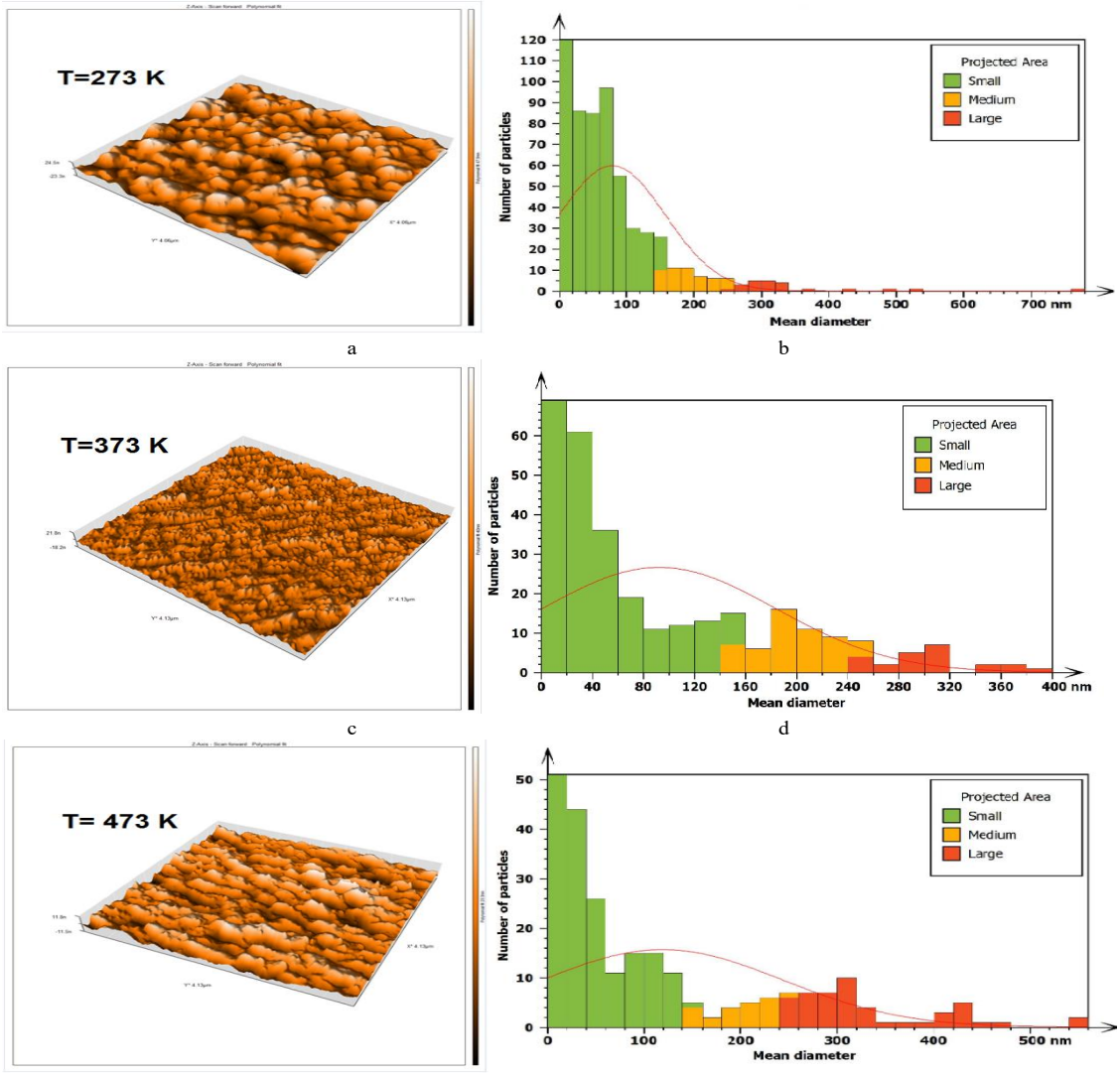

FIGURE 5a,b,c,d,e,f. AFM image for $ZnTe_{0.8}Se_{0.2}$ thin films at R.T, 373. and 473 K

Figure 5 illustrates the AFM scans of ZTS thin films at R.T., 373 K, and 473 K temperatures. The aforementioned pictures demonstrate how efficiently distributed and free of islands and pinholes the film is. It contains a lot of columnar grains

TABLE 3. Average roughness, grain size, and ZTS thin films' root mean square at (R.T, 373, and 473) K

Thickness (500 nm)	Grain size (nm)	Surfaces roughness (nm)	Root mean square (nm)
R. T	78.59	19.45	27.14
373	92.23	21.67	28.22
473	99.12	23.13	30.73

CONCLUSION

This study came to several conclusions: preparation of ZnTe0.8Se0.2 thin films via thermal evaporation are possible, all films had allowed direct transition electronic and as annealing temperatures increased, the energy gap decreases from (1.86 to 1.78) eV, suggesting that they are appropriate for forming a junction in a solar cell. As annealing temperatures climbed, the transmittance and absorption peak of the curve shifted toward photon energies, suggesting more absorbency. In the visible region, the refractive index falls while the extinction coefficient rises as a result of an increasing absorption coefficient, indicates improved optical properties in this region for photovoltaic applications. The XRD patterns illustrate its cubic crystal arrangement and polycrystalline nature, with the (111) plane serving as the preferred orientation. The spectra curve moved less toward low angle diffraction values when the annealing temperature was elevated with the appearance of an increase in the values of crystal size and grain size of the samples.

ACKNOWLEDGMENTS

We thank the Thin Film Lab., Department of Physics / College of Education for Pure Science /Ibn Al-Haitham, University of Baghdad.

REFERENCES

1. Hassanien, A., Aly, K., & Akl, A. A. (2016). Study of optical properties of thermally evaporated ZnSe thin films annealed at different pulsed laser powers. Journal of Alloys and Compounds, 685, 733-742. https://doi.org/10.1016/j.jallcom.2016.06.180.
2. BENSIRADJ, N. E., YOUSFI, H., BENSIRADJ, T., & OUAMERALI, O. (2022). Theoretical investigation of the spectroscopic properties of ZnTe, ZnTe, and ZnTe-systems. https://doi.org/10.21203/rs.3.rs-1879560/v1.
3. Gromboni, M. F., & Mascaro, L. H. (2016). Optical and structural study of electrodeposited zinc selenide thin films. Journal of Electroanalytical Chemistry, 780, 360-366. https://doi.org/10.1016/j.jelechem.2016.04.037.
4. Khan, T. M., Mehmood, M. F., Mahmood, A., Shah, A., Raza, Q., Iqbal, A., & Aziz, U. (2011). Synthesis of thermally evaporated ZnSe thin film at room temperature. Thin Solid Films, 519(18), 5971-5977. https://doi.org/10.1016/j.tsf.2011.03.045
5. Hile, D. D., Swart, H. C., Motloung, S. V., & Koao, L. F. (2022). Zinc selenide semiconductor: Synthesis, properties and applications. Nanoscale Compound Semiconductors and their Optoelectronics Applications, 67-84. https://doi.org/10.1016/b978-0-12-824062-5.00001-4.
6. Hassun, H. K., Hussein, B. H., Al-Maiyaly, B. K., Moussa, Y. K., Shaban, A. H., & Jasim, K. A. (2025). Impact thickness on performance of higher quality ZnTe photodetectors. AIP Conference Proceedings, 3321, 020018. https://doi.org/10.1063/5.0289998.
7. Yadav, B. K., Singh, P., Yadav, C. P., Pandey, D. K., & Singh, D. (2020). Structural and wavelength dependent optical study of thermally evaporated Cu₂Se thin films. Zeitschrift für Naturforschung A, 75(9), 781-788. https://doi.org/10.1515/zna-2020-0098.
8. K. Al Abdullah, F. Al Alloush, A. Jaafar, and C. Salame, "Investigation of the monocrystalline silicon solar cell physical behavior by AC impedance spectra," Energy Procedia 57, (2014). https://doi.org/10.1080/01411594.2021.1932884.
9. Răduță, A., Panaitescu, A., Manica, M., Iftimie, S., Antohe, V., Toma, O., Radu, A., Ion, L., Suchea, M. P., & Antohe, Ș. (2024). Effect of deposition working power on physical properties of RF-sputtered CdTe thin films for photovoltaic applications. Nanomaterials, 14(6), 535. https://doi.org/10.3390/nano14060535.
10. Ali, G. A., Moustafa, S. H., Amer, M. I., Shaban, H., Emam-Ismail, M., Shaaban, E. R., & El-Hagary, M. (2021). Effect of CU incorporation on optoelectronic properties of E-BEam evaporated ZnO thin films by Ellipsometric investigations. https://doi.org/10.21203/rs.3.rs-294805/v1.
11. Horoz, B., Tuna Yıldırım, S., Soltabayev, B., Ateş, A., Acar, S., & Yıldırım, M. A. (2024). Effect of SILAR cycle on gas sensing properties of In2O3 thin films for CO gas sensor. Journal of Materials Science: Materials in Electronics, 35(2). https://doi.org/10.1007/s10854-024-11970-5.

12. Hankare, P., Jadhav, B., Garadkar, K., Chate, P., Mulla, I., & Delekar, S. (2010). Synthesis and characterization of nickel selenide thin films deposited by chemical method. Journal of Alloys and Compounds, 490(1-2), 228-231. https://doi.org/10.1016/j.jallcom.2009.09.132.
13. Bruno, A., Herlina, A., Erdenebileg, E., Li, J., Wang, H., Mathews, N., & Mhaisalkar, S. (2021). Design of versatile and ultra-stable Co-evaporated perovskites solar cells and minimodules. Proceedings of the International Conference on Perovskite Thin Film Photovoltaics and Perovskite Photonics and Optoelectronics. https://doi.org/10.29363/nanoge.nipho.2022.014.
14. Sudarshan, C., Jayakumar, S., Vaideki, K., & Sudakar, C. (2020). Te-rich Bi2Te3 thin films by electron−beam deposition: Structural, electrical, optical and thermoelectric properties. Thin Solid Films, 713, 138355. https://doi.org/10.1016/j.tsf.2020.138355.
15. Abdulateef, A.N., Alsudani, A., Chillab, R.K., Jasim, K.A., Shaban, A.H., Calculating the mechanisms of electrical conductivity and energy density of states for Se85Te10Sn5-xInx glasses materials, Journal of Green Engineering, 2020, 10(9), pp. 5487–5503.
16. Emam-Ismail, M., El-Hagary, M., Shaaban, E., & Al-Hedeib, A. (2012). Microstructure and optical studies of electron beam evaporated ZnSe1−xTex nanocrystalline thin films. Journal of Alloys and Compounds, 532, 16-24. https://doi.org/10.1016/j.jallcom.2012.04.013.
17. Craciun, V., Cristea, D., Socol, G., Lambers, E., Trusca, R., Fairchild, S., Back, T., Gruen, G., & Craciun, D. (2016). Characteristics of LaB6 thin films grown by pulsed laser deposition. Journal of Vacuum Science & Technology A: Vacuum, Surfaces, and Films, 34(5). https://doi.org/10.1116/1.4960647.
18. Adav, B. K., Singh, P., Yadav, C. P., & Pandey, D. K. (2021). Synthesis and characterization of znse_{1-x}Te_x thin films. Phase Transitions, 94(5), 326-337. https://doi.org/10.1080/01411594.2021.1932884.
19. M. Ali, S. M., Shehab, A. A., & Maki, S. A. (2018). Effect of CU doping on the electrical properties of ZnTe by vacuum thermal evaporation. Ibn AL-Haitham Journal for Pure and Applied Sciences, 31(3), 20-25. https://doi.org/10.30526/31.3.2023.
20. Khanlary, M., Rahmani, E., Pasalari, Z., & Reyhani, A. (2024). Post-annealing effect on the structural and optical properties of tungsten oxide thin films prepared by thermal evaporation. https://doi.org/10.2139/ssrn.4903454.
21. Samir A. Maki Hanan K. Hassun. The structural and optical properties of zinc telluride thin film by vacuum thermal evaporation technique. Ibn Al-Haitham J for Pure & Appl Sci [Internet]. 2016 May 8;29 (2):1–12. Available from: https://www.researchgate.net/publication/327920438
22. Soud, A. J., & Al-Maiyaly, B. K. (2024). Influence of annealing temperature on nano crystalline description for CuZnS thin films. Chalcogenide Letters, 21(5), 385-394. https://doi.org/10.15251/cl.2024.215.385.
23. Salih AA. The Structural and Surface Morphology Properties of Aluminum Doped CdO Thin Films Prepared by Vacuum Thermal Evaporation Technique. Ibn Al-Haitham Jour for Pure & Appl Sci [Internet]. 2014 Sep 8;27 (2):1–13. Available from: https://www.researchgate.net/publication/284456533.
24. Salih AA, Abad WK, Fadaam SA, Hussein BH. Fabrication of lead oxide nanoparticles by green synthesis method for photovoltaic applications. Dig J Nanomater Biostruct. 2023 Dec 1;18(4):1225–33.
25. Ahmed, B.A., Mohammed, J.S., Fadhil, R.N., ...Shaban, A.H., Al Dulaimi, A.H., The dependence of the energy density states on the substitution of chemical elements in the Se6 Te4-xSbx thin film, Chalcogenide Letters, 2022, 19(4), pp. 301–308.
26. Aleabi, S. H., Watan, A. W., Salman, E. M., Jasim, K. A., Shaban, A. H., & AlSaadi, T. M. (2018). The study effect of weight fraction on thermal and electrical conductivity for unsaturated polyester composite alone and hybrid. AIP Conference Proceedings, 1968, 020019. https://doi.org/10.1063/1.5039178.
27. Bao X, Xue J, Yang X, Liu J, Yang H, Tang Z, et al. Preparation and optimization of all-inorganic CdSe/ZnTe solar cells. Science Direct [Internet]. 2024 Aug 1; Volume 272,1–20. Available from: https://ssrn.com/abstract=4717572
28. Zainab, J., Jasim, K. A., Kadhum, F. J., & Shaban, A. H. (2021). Heat treatment at different temperatures and its effect on the optical properties of pure PMMA and PMMA-coumarin. Key Engineering Materials, 900, 42-47. https://doi.org/10.4028/www.scientific.net/kem.900.42.
29. Ali, R. M., & Najim, F. A. (2024). Depending the structural and optical properties of ZnTe thin films on cd doping by thermal evaporation. Al-Qadisiyah Journal of Pure Science, 29(2). https://doi.org/10.29350/2411-3514.1282).